Determining local magnetic susceptibility tensors in paramagnetic lanthanide crystalline powders from solid-state NMR chemical shift anisotropies

Ridvan Ince, Abdelatif Doudouh, Nicolas Claiser, Eric Furet, Thierry Guizouarn, Laurent Le Pollès, Gwendal Kervern

Determining local magnetic susceptibility tensors in paramagnetic lanthanide crystalline powders from solid-state NMR chemical shift anisotropies

Ridvan Ince,[†] Abdelatif Doudouh,[†] Nicolas Claiser,[†] Laurent Le Pollès,[‡] Thierry Guizouarn,[¶] Éric Furet,[‡] and Gwendal Kervern[*,†]

[†]*Université de Lorraine, UMR 7036 (UL-CNRS) CRM2, BP 70239 Boulevard des Aiguillettes, F 54506 Vandœuvre-lès-Nancy, France.*

[‡]*ENSCR, UMR 6226 (UL-CNRS) École Nationale Supérieure de Chimie de Rennes, Campus de Beaulieu - Bâtiment 10B, F 35042 Rennes Cedex, France.*

[¶]*ISCR, UMR 6226 (UL-CNRS) Université de Rennes 1, Campus de Beaulieu - Bâtiment 10B, F 35042 Rennes Cedex, France.*

E-mail: gwendal.kervern@univ-lorraine.fr

Phone: +33 3 72 74 56 73

Abstract

Exploring magnetic properties at the molecular level is a challenge that have been met by developing many experimental and theoretical solutions such as polarized neutron diffraction (PND), muon-spin rotation (μ-SR), electron paramagnetic resonance (EPR), SQUID-based magnetometry measurements and advanced modelling on open-shell systems and relativistic calculations. These methods are powerful tools that shed light on the local magnetic response in specifically designed magnetic materials such as contrast agents, for MRI, molecular magnets, magnetic tags for biological NMR etc.

All of these methods have their advantages and disadvantages. In order to complement the possibilities offered by these methods, we propose a new tool that implements a new approach combining simulation and fitting for high-resolution solid-state NMR spectra of lanthanide-based paramagnetic species.

This method relies on a rigorous acquisition thanks to Short Highpower Adiabatic Pulses (SHAP) of high-resolution solid-state NMR isotropic and anisotropic data on a powdered magnetic material. It is also based on an efficient modelling of this data thanks to a semi-empirical model based on a parametrization of the local magnetism and the crystal structure provided by diffraction methods. The efficiency of the calculation relies on a thorough simplification of the electron-nucleus interactions (point-dipole interaction, no Fermi-contact) which is validated by experimental analysis.

By taking advantage of the efficient calculation possibilities offered by our method, we can compare a great number of simulated spectra to experimental data and find the best-matching local magnetic susceptibility tensor. This method was applied to a series of isostructural lanthanide oxalates which are used as a benchmark system for many analytical methods. We present the results of thorough solid-state NMR and extensive modelling of the hyperfine interaction (including up to 400 paramagnetic centers) that yields local magnetic susceptibility tensors measurements that are self-consistent as well as consistent with bulk susceptibility measurements.

Introduction

Getting information on magnetic susceptibility at a molecular level requires a probing particle that is sensitive to the local magnetization and can get close to the probed magnetic center. The analytical techniques associated to such probes are (polarized) neutron diffraction (PND)[1–3], muon spin rotation (μ-SR)[4,5] or electron paramagnetic resonance (EPR)[6,7].

NMR-active nuclei surrounding magnetic centers in various materials have also been used to extract structural information from the local magnetic properties[8–11]. However,

local magnetic structure probing by solid-state NMR has remained scarce so far[12–14]. Some recent studies have been focusing on information on local magnetic susceptibility tensors from solid-state NMR data[15,16] or electronic spin density[17,18] but they do not exploit the full extent of the chemical shift anisotropy in the models they develop.

Most of these methods can give relative values for the anisotropy in the local magnetic susceptibility tensor, but in order to achieve the goal of getting both the principal values and the orientation of the local magnetic tensor in the crystal frame, one must work with strong constrains on the crystal size of the studied sample and/or ultra-low temperatures.

In this study we propose to rationalize the use of spin 1/2 NMR-active nuclei as probes for determination of local magnetic properties in microcrystalline powders. We propose to couple a range of thoroughly tested and calibrated broadband solid-state NMR experiments with a magnetic point-dipole fast-calculation approach that allows to test a great number of local magnetic structures in search of the best agreement with the experimental data.

Using nuclear magnetic moment as a probe for local magnetism is not straightforward though: solid-state NMR of paramagnetic substances remains a challenging topic in many ways. Experimental complexity arises from the unusual chemical shift and shift anisotropy ranges, fast-relaxation inducing phenomena, and strong bulk magnetic susceptibility (BMS) broadening[19]. Obtaining reliable spectra remains a challenging task. However, using very-fast and ultra-fast magic-angle spinning hardware opened new possibilities, reinforced by developments of adiabatic methods in solid-state NMR[20,21].

We applied the most recent developments of solid-state NMR methodology to a series of lanthanide oxalate complexes $[Ln_2(C_2O_4)_3]$, 9.5 H_2O (Ln=La **(1)**, Ce **(2)**, Pr **(3)** and Nd **(4)**). These complexes appear in many studies and their synthesis and properties are very well known. They form a bi-dimensional metal-organic framework for which each lanthanide shares 3 oxalates with its neighbours and completes its coordination sphere with water molecules[22] (figure 1).

In this study, we demonstrate the use of ^{13}C NMR as a local magnetic probe for the study

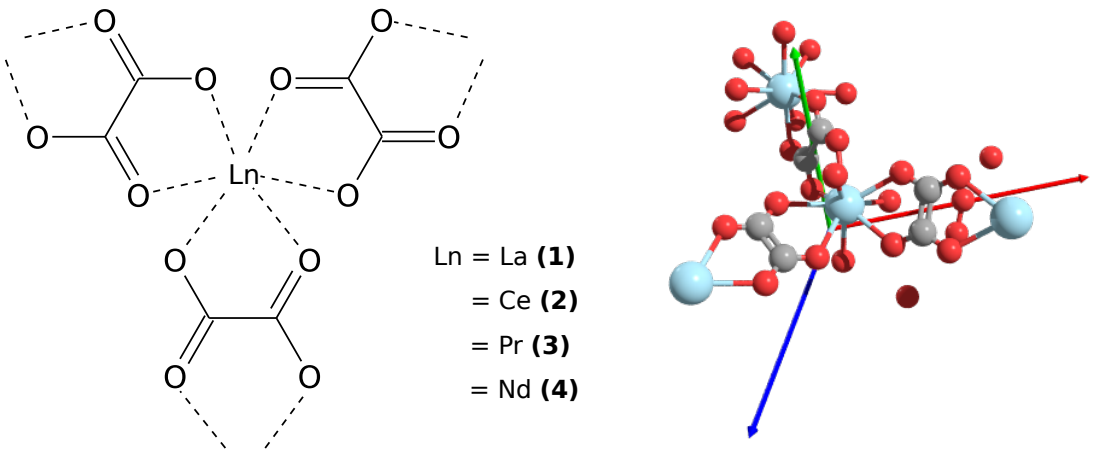

Figure 1: Chemical structure (water molecules have not been drawn for clarity) and crystal structure (hydrogen have not been represented for the same reason) of $[Ln_2(C_2O_4)_3]$, 9.5 H_2O. The compounds **(1)** to **(4)** have isostructural crystal structures.

of lanthanide compounds. ^{13}C NMR isotropic and anisotropic data combined with a point-dipole simulation of magnetic interactions within the crystal frame gives a full description of the local magnetic susceptibility tensor.

This method, based on solid-state NMR under magic angle spinning of a microcrystalline powder, requires a previous knowledge of the crystal structure and achieves a full characterization of the local magnetic susceptibility tensor in the crystal frame.

Methods

Experimental details

Synthesis of crystalline powders of $[Ln_2(C_2O_4)_3]$, 9.5 H_2O

All lanthanide oxalates where synthesized by diffusion in an agarose gel in a test tube at 50°C temperature. More details about the crystal growth can be found in the supplementary information[23].

NMR experiments

All NMR experiments were performed on a 300 MHz Bruker Avance III HD spectrometer equipped with a 4 mm triple resonance probe. Acquisition of NMR data on $[La_2(C_2O_4)_3]$, $9.5H_2O$ was performed under cross-polarization at 2 kHz MAS speed (CPMAS), with 100 kHz heteronuclear decoupling (SPINAL 64[24]) with a recycling delay D1 of 10s.

For the paramagnetic samples $[Ce_2(C_2O_4)_3]$, $9.5H_2O$ and $[Nd_2(C_2O_4)_3]$, $9.5H_2O$, we performed direct acquisition without decoupling under controlled temperature, with short excitation hard pulse (1 μs) and a short highpower adiabatic (SHAP)[25] double spin echo under 8 kHz MAS. We did the same type of experiment with $[Pr_2(C_2O_4)_3]$, $9.5H_2O$ under 12.5 kHz MAS. For all compounds, the D1 recycle delay was set to 250 ms. The temperature regulation was set to 278 K which, according to prior calibration with lead nitrate, means that the inside of the rotor was at 289K. The chemical shifts were calibrated with respect to TMS using adamantane as a secondary reference (^{13}C shifts of 29.45 and 38.48 ppm).

Temperatures in the rotor were calibrated prior to the experiment by measuring ^{207}Pb chemical shifts in a lead nitrate sample under controlled temperature and MAS spinning speed.[26]

Quality assessment of NMR measurements

In order to achieve accurate measurements of the local magnetic susceptibility tensor, we had to ensure that the quality of the MAS NMR spectra was optimum given the difficulties inherent to the acquisition of NMR data over spectral width wider than 100 kHz.

Our first problem was to make sure that the response of our NMR probe was accurate over the whole bandwidth of our experiments. In order to verify this, we acquired a series of MAS spectra under the same conditions as that of the measurements on paramagnetic lanthanide oxalates, but making several acquisitions with various carrier frequency in order to check that the peak intensities were not affected on the edge of the acquisition window (see SI). This also ensured that our very short excitation hard pulse (1 μs) was not cut by

the probe response over the whole spectral window.

In order to get rid of baseline distortions due to very short dwell time compared to the probe's ringdown time, we used a double spin echo to allow for probe-circuit ringdown before the start of acquisition on the peak of the FID. However, since it is documented that the shortest inversion pulses possible on our hardware (about 6.25 μs) are not efficient over such bandwidth, we used a couple of short highpower adiabatic pulses (SHAP) to achieve proper inversion over the full spectrum bandwidth[25]. We assessed the quality of the inversion by performing inversion-recovery experiments with various SHAPs and finding the best conditions for a full-bandwidth inversion (see SI).

We also had to ensure that the magic angle spinning was neither too fast nor too slow to get the best quality for chemical shift anisotropy measurements. Hodgkinson and Emsley proposed to establish a quality criterion for chemical shift anisotropy determination under magic angle sample spinning[27]. They show that for anisotropy determination, magic angle sample spinning rates between 0.15 and 0.5 times the chemical shift anisotropy ($0.15\delta \times \nu_0 \leq \nu_{MAS} \leq 0.5\delta \times \nu_0$ where $\delta = \delta_{zz} - \delta_{iso}$ is the anisotropy parameter and ν_0 the Larmor frequency) give better results for the determination of δ than a static sample. However, they also claim that for the asymmetry parameter determination ($\eta = (\delta_{yy} - \delta_{xx})/\delta$), nothing is better than a static sample.

In order to try and maximize the precision of our experimental data, we made a compromise between the two criteria proposed by Hodgkinson and Emsley. We also had to take into account the extra difficulty posed by bulk magnetic susceptibility broadening[19] which must be overcome in order for the sidebands not to overlap. We set our MAS frequency to match for the lower range of the criterion for accurate anisotropy determination $\nu_{MAS} \geq 0.15\delta \times \nu_0$ while ensuring that spinning sideband were not overlapping ($\nu_{MAS} > 2\times$ full width at half height).

X-Ray diffraction measurements

The isostructurality of all the lanthanides was verified thanks to X-Ray diffraction measurements on powdered samples. The diffractograms were acquired on an Xpert Pro Pan-Analytical diffractometer and can be found in the supplementary information material.

Magnetic susceptibility measurements

Magnetic susceptibility measurements were carried out using a MPMS XL-5 Quantum Design SQUID magnetometer. The detailed measurements are available in the supplementary information material.

Computation of diamagnetic contribution to chemical shift tensors

NMR parameters have been computed on the $[La_2(C_2O_4)_3]$, 9.5 H_2O crystalline phase. Calculations have been performed within the Gauge Including Projected Augmented Wave formalism[28,29] as implemented in the CASTEP program, version 20.[30] The PBE exchange and correlation functionals,[31] on-the-fly generated ultrasoft pseudopotentials, an expansion of the plane-wave basis sets up to an energy cutoff of 1100 eV, and a sampling of the Brillouin zone up to $6 \times 6 \times 6$ k-points grid have been used. Tests concerning the convergence of NMR parameters with respect to energy cutoff and k-point sampling are reported in the SI.

Model and approximations

Predicting solid-state NMR chemical shift parameters in paramagnetic systems can be performed with several methods presenting different level of approximation ranging from a very quick point-dipole approximation of the hyperfine shift to a complete ab-initio calculation of contact, dipolar, and paramagnetic spin-orbit (PSO) contribution of the unpaired electrons spins to the paramagnetic shift. The latter method can give extremely precise results but requires a huge amount of computational power in order to get one solid-state NMR spectrum.[10,32–34]

Since it is based on the search of an optimal agreement between experimental data and theoretical predictions, the method we want to present here requires to calculate a large number of paramagnetic solid-state NMR spectra on the basis of the local chemical and magnetic structures.

While the local chemical structure is accessible by X-Ray diffraction in crystalline materials, the local magnetic structure has to be either postulated, calculated (ab-initio or from macroscopic measurements data) or measured with heavy equipment with methods such as PND or $\mu-$SR.

In this study, we postulate a shape for the local magnetic structure based on the 6 free parameters of the local magnetic susceptibility rank-2 tensor. The susceptibility tensor $\mathbb{X}_0$ of the asymmetric unit is parametrized, and the tensors $\mathbb{X}_j$ for all the other paramagnetic centers in the crystal are deduced from the symmetry operations within the crystal space group.

Once the magnetic susceptibility tensors within the crystal have been parametrized, we used the semi-empirical point-dipole approximation for the fast-calculation of NMR spectra. In this model, we calculate the hyperfine interaction between each NMR observable nucleus in the asymmetric unit of the crystal structure and an ensemble of magnetic point dipoles generated by crystal symmetry operations (multiple cells) and for which the magnetic moment is driven by the magnetic susceptibility tensor.

The terms that are neglected in this model are:

- the contact terms, that would come in the case of delocalized magnetic moments rising from nd or $5f$ orbitals. The case of delocalization in $4f$ orbitals is rare and requires very high symmetry around lanthanide atoms[35]

- the multipolar terms that would come from a diffuse point-dipole that could arise from either lanthanide mobility[36] or from diffuse nd or $5f$ orbitals[16].

In this case, these approximations are justified by several aspects of the problem:

- the absence of contact shift is justified by the fact that spin delocalization is rare in lanthanide complexes and requires a high D_3 symmetry in order for the contracted $4f$ orbitals to have a contribution in the molecular orbitals[35]. Such high symmetry is not present here.

- the lanthanide oxalates that we study are metal-organic frameworks in which atomic mobility is not observed. This is supported by both X-Ray Diffraction and NMR data.

- finally, since we study nuclei that are not directly bonded to the metal center[11,20] and if we consider the ionic radius of lanthanides in general[37], we are considering nuclei that are at a distance from the magnetic center that is about 3 times the maximum possible extension of the $4f$ orbitals. Several publication[16,36] showed that this situation is virtually indistinguishable from the point dipole approximation.

Consequently, in this model, for a given crystal containing n inequivalent NMR-active nuclei in the asymmetric unit, the chemical-shift Hamiltonian will come up as a sum of two terms: one originating from diamagnetism, that will be considered as identical for each compound of this series of lanthanide oxalate, and a second term originating from the paramagnetic interaction between the observed nucleus and all of the surrounding paramagnetic centers. The Hamiltonian for the nucleus i can be summarized as:

$$\mathcal{H}_i^{CS} = \mathcal{H}_i^{dia} + \mathcal{H}_i^{para} \tag{1}$$

where $\mathcal{H}_i^{dia}$ is the diamagnetic contribution to the chemical shift that can either be inferred from experimental measurements on isostructural diamagnetic equivalents or calculated ab-initio, and $\mathcal{H}_i^{para}$ is the paramagnetic contribution to the chemical shift Hamiltonian that can again be separated in two chemical-shift like terms: one originating from the contact interaction, the other coming from the dipolar interaction between the electrons and the observed nucleus.

$$\mathcal{H}_i^{para} = \mathcal{H}_i^C + \mathcal{H}_i^D \tag{2}$$

The contact Hamiltonian for the nucleus i can be written as:

$$\mathcal{H}_i^C = \overrightarrow{I}_i \cdot \sum_j \mathcal{A}_{ij} \mathbb{X}_j \cdot \overrightarrow{B}_0 \tag{3}$$

where $\overrightarrow{I}_i$ are the nuclear spin vectors, $\overrightarrow{B}_0$ the local magnetic field, the average local magnetic moment of each paramagnetic center j in the crystal is given by $\langle \mu_j \rangle = \mathbb{X}_j \overrightarrow{B}_0$ and the coupling constant between the nucleus and each paramagnetic center in its direct chemical vicinity is noted $\mathcal{A}_{ij}$. In this situation, two paramagnetic centers are only two bonds away from the carbons. However, as we explained earlier, we placed ourselves in a situation where we expect this term to be negligible when compared to the dipolar term. This statement is backed up by experimental evidence and it is discussed in the discussion section at the end of this paper.

As stated earlier, the dipolar contribution will be considered as originating from an ensemble of point-dipoles in the crystal lattice. The hyperfine Hamiltonian for the nucleus i surrounded by an ensemble of j paramagnetic centers becomes:

$$\mathcal{H}_i^{para} = \frac{\mu_0 \gamma_I}{4\pi} \sum_j \frac{1}{r_{ij}^3} \left[3 \frac{\left(\overrightarrow{I_i} \cdot \overrightarrow{r_{ij}} \right) \left(\mathbb{X}_j \overrightarrow{B}_0 \cdot \overrightarrow{r_{ij}} \right)}{r_{ij}^2} - \overrightarrow{I_i} \cdot \mathbb{X}_j \overrightarrow{B}_0 \right] \tag{4}$$

where $\overrightarrow{I}_i$ and $\overrightarrow{B}_0$ have been described earlier and the relative positions $\overrightarrow{r}_{ij}$ and local magnetic susceptibility tensors $\mathbb{X}_j$ of the paramagnets j are generated through the symmetry operations of the crystal applied to the asymmetric unit.

Both terms $\mathcal{H}_i^C$ and $\mathcal{H}_i^D$ are proportional to the externa field via an anisotropy tensor. Again, we consider that the contact term is weak and we do not take it into account in our calculation. We have to treat the sum of dipolar terms which can be decomposed in a series of rank 2 tensor operators out of which the non-secular terms can be neglected. Since

both paramagnetic and diamagnetic terms can be simplified this way, we can factorize the approximated chemical shift Hamiltonian:

$$\mathcal{H}_i^{CS} = (\Delta_{dia}^i + \Delta_{para}^i)\gamma_I B_0 I_{i_z} \tag{5}$$

where $\Delta_{total}^i = \Delta_{dia}^i + \Delta_{para}^i$ is the full chemical shift anisotropy tensor of the i^{th} nucleus. Δ_{dia}^i is the chemical shift rank-2 tensor of the diamagnetic analog of the i^{th} nucleus and Δ_{para}^i is the paramagnetic contribution and can be calculated thanks to the hypothesis mentioned earlier[38]:

$$\Delta_{para}^i = \frac{1}{4\pi}\sum_j \frac{1}{r_{ij}^5}\left[3\begin{pmatrix} x_{ij}^2 & x_{ij}y_{ij} & x_{ij}z_{ij} \\ x_{ij}y_{ij} & y_{ij}^2 & y_{ij}z_{ij} \\ x_{ij}z_{ij} & y_{ij}z_{ij} & z_{ij}^2 \end{pmatrix} - r_{ij}^2\mathbb{1}\right]\cdot\mathbb{X}_j \tag{6}$$

we used the notation $\mathbb{1}$ for the 3×3 identity matrix. The resulting tensor can be symmetrized as the rank-1 tensor terms that may come out of this expression are not directly observable in NMR[39].

The Δ_{dia}^i chemical shift tensor was evaluated thanks to a CPMAS spectrum of the isostructural diamagnetic compound **(1)** at low spinning speed. We used the ssNake software for sideband pattern fitting.[40] This analysis gave the principal values of the diamagnetic chemical shift tensor, its orientation for each of the 3 carbons in the asymmetric unit was then evaluated with DFT calculation using the CASTEP software[30].

The magnetic susceptibility rank-2 tensor in the asymmetric unit ($\mathbb{X}_0$) was parametrized with up to 6 independent orthogonal parameters. In order to give perfectly random starting points for our optimum searches we chose to decompose the $\mathbb{X}_j$ tensors into their spherical tensor components:

$$\mathbb{X}_0 = \chi_{iso}(T)\left(\mathbb{1} + \sum_{p=-2}^{+2} a_2^p \mathbf{T}_2^p\right) \tag{7}$$

where $\chi_{iso}(T)$ and a_2^p are the 6 free parameters of our model and $\mathbb{1}$ and $\mathbf{T}_2^p$ are respectively the identity matrix and the 5 normalized rank-2 tensor operators. χ_{iso} is left as a free parameter

in our model but it can be evaluated independently by measuring the macroscopic magnetic susceptibility of the studied sample thanks to SQUID measurements. We will show that leaving this parameter free gives a result in perfect agreement with SQUID measurements.

The number of free parameters a_2^p for the sphere deformation depends on the position of the paramagnetic center in the unit-cell. If the magnetic center is on a specific Wickoff position, the amplitude terms for the spherical harmonics that do not respect the local symmetry must be set to zero. In the case presented in this study, the lanthanide positions are not constrained by local symmetry and the parametrization of the local magnetic susceptibility tensors therefore take 6 free parameters.

The paramagnetic centers used in this calculation fall within a distance r_{ij} from the observed nucleus. In order to optimize the calculation time, the cutoff radius for the r_{ij} distances was evaluated prior to any optimum calculation by choosing a random local susceptibility tensor with an estimation of the isotropic value based on the Curie Law. A series of spectra was calculated with an increase in the cutoff radius up to the point where two consecutive calculated spectra did not differ from more that 0.1% at the maximum. For **(2)** the cutoff radius was set to 10Å, and for **(3)** and **(4)**, due to higher isotropic susceptibility, it was set to 20Å(see SI for convergence method). This calculation therefore implies to take into account about 480 paramagnetic centers, and can be performed within a few seconds on a desktop computer.

The calculated chemical shift tensors are thus used to simulate a solid-state NMR spectrum that is compared to the experimental data. The quality of the model is evaluated by minimizing the standard deviation between the simulated and experimental spectra.

While a single fit can give a single tensor value for the local magnetic susceptibility that is in perfect agreement with the observed NMR spectrum, we took advantage of the rapidity of this calculation to estimate the error on each of the 6 free parameters of the local magnetic susceptibility tensor with a Monte-Carlo procedure that repeats the fitting process with added noise in the model.

The quality of each fit was evaluated by comparing the standard deviation obtained with that of a pure-noise spectrum generated randomly with the same distribution characteristics as the experimental noise. The detail of the error determination procedure can be found in the SI.

Results

Magnetic susceptibility tensors

We acquired our spectra under 8 kHz MAS for compounds **(2)** and **(4)**, as they presented narrower line than **(3)**. The resulting spectra are presented in figure 2 and show the actual bandwidth that was necessary for such acquisition (ca 1500 ppm at 75.49 MHz $\approx$ 120 kHz). Such spectral width is well within the probe's 90% response bandwidth (see supplementary information).

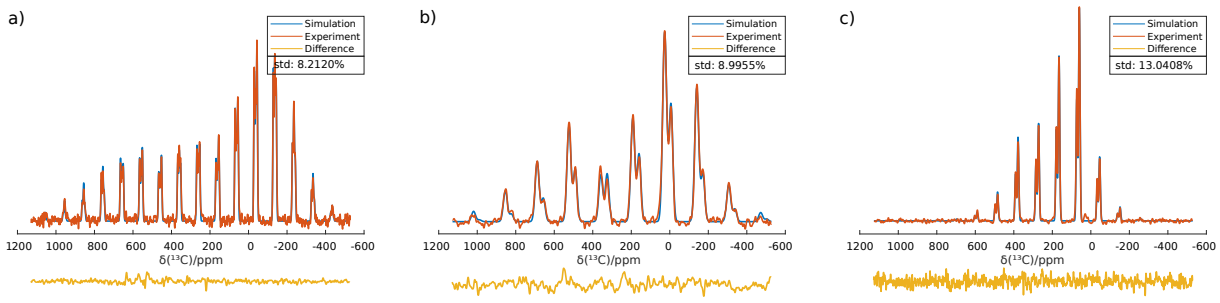

Figure 2: Fitting of the experimental data for a) $[Ce_2(C_2O_4)_3]$, $9.5H_2O$, b) $[Pr_2(C_2O_4)_3]$, $9.5H_2O$ and c) $[Nd_2(C_2O_4)_3]$, $9.5H_2O$. Experimental data (in red) and the best fit (in blue) are superimposed on top of the figure, and the differences between the fit and the data (in yellow) are presented at the bottom.

Our fitting procedures were applied to the MAS NMR spectra of **(2)** to **(4)**. It uses as an input the diamagnetic CSA obtained from **(1)**. The results of the optimal fits are presented in figure 2. There are some discrepancies between the experiment and the best fit for the cerium oxalate, but the differences between the experiments and the best-fit simulations on praseodymium and neodymium cannot be distinguished from the noise in the NMR data.

Each of these fits correspond to an optimized magnetic susceptibility tensor according to our fast-calculation method. It inputs the crystal structure obtained from X-Ray diffraction on our samples and the chemical shift tensors extracted from experimental data on the diamagnetic isostructural compound **(1)**.

Error analysis

The error on the tensor parameters was evaluated by repeating the fitting procedure 500 times with 500 different sets of noise added to the model spectrum. Each set of noise was generated randomly with amplitude and spectral characteristics that are identical to that of the noise in the processed experimental spectra. We used an orthonormal base for the parametrization of the local magnetic susceptibility tensor. Since we obtain a set of normally distributed values for each of the 6 parameters (as can be seen in table 1 as well as in figure 9 of the supplementary information) it shows the consistency of our model: there are no more than one local minimum in the root-mean square deviation function described in the orthonormal basis of the local magnetic susceptibility tensor's parameter space.

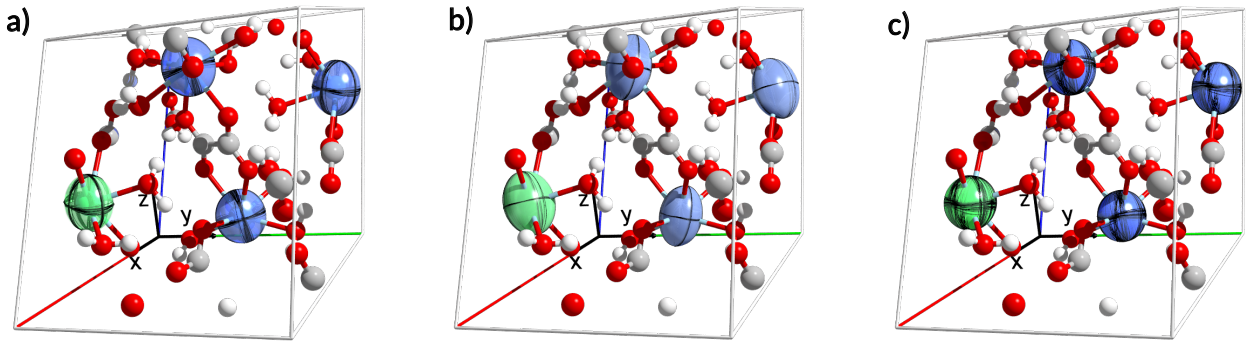

Figure 3: Error analysis for the local magnetic susceptibility tensor for: a) $[Ce_2(C_2O_4)_3]$, 9.5 H_2O, b) $[Pr_2(C_2O_4)_3]$, 9.5 H_2O and c) $[Nd_2(C_2O_4)_3]$, 9.5 H_2O. This figure represents a bundle of tensors obtained after adding noise to the model. Each of the 500 optimization processes gave an ensemble of 500 sets of spherical harmonics terms a_2^p (see equation 7) that correspond to each tensor represented here. The numerical value and errors are presented in table 1.

As can be seen on table 1, each of the parameters fitted with this procedure shows a

normal distribution of values with standard deviation not exceeding 5% of the isotropic values for magnetic susceptibility. The resulting bundles of tensors are therefore extremely consistent, and a Euler representation of the tensor bundle's parameters show an extremely narrow distribution of the α and β Euler angles, as well as anisotropy parameters (see supplementary information for Euler representation of tensor bundles and sensitivity to each parameter variation).

Table 1: Values and errors on the fitting parameters for each compound. The harmonic terms a_2^p are in % of the isotropic susceptibility, which is itself in m^3. For each parameter, the average value μ as well as the standard deviation σ are given. A graphical version of this table can be found in the supplementary information

Compound	$[Ce_2(C_2O_4)_3]$, $9.5H_2O$		$[Pr_2(C_2O_4)_3]$, $9.5H_2O$		$[Nd_2(C_2O_4)_3]$, $9.5H_2O$	
Parameter	μ	σ	μ	σ	μ	σ
$\chi_{iso}(\times 10^{-32}\,\mathrm{m}^3)$	4.769	0.01	9.965	0.04	10.36	0.03
$a_2^0(\%\chi_{iso})$	5.08	0.25	9.73	0.44	2.10	0.20
$a_2^1(\%\chi_{iso})$	0.38	0.47	8.14	1.51	1.45	0.37
$a_2^{-1}(\%\chi_{iso})$	−2.08	0.91	10.00	2.13	−0.42	0.79
$a_2^2(\%\chi_{iso})$	−3.90	0.15	1.40	0.41	−1.04	0.13
$a_2^{-2}(\%\chi_{iso})$	5.99	1.61	−4.52	4.91	0.52	1.25

Analyzing the case of compound **(4)** in the light of Euler representation might seem to stand out as a dark spot on this beautiful picture. However, one needs to remark that the local magnetic susceptibility tensor is almost spherical in this case (most terms in the spherical harmonics decompositions are less than 2% of the isotropic value), and it is therefore unlikely to have a well-defined principal axis system as the local χ tensor is almost spherical.

The consistency of the magnetic susceptibility tensor bundles strongly advocates for the unicity of the solution found by our method for the search of the local magnetic structure while given crystallographic data and solid-state NMR spectra. However, the consistency with other magnetic measurements needs to be tested.

Discussion

Experimental evidence for the negligible contribution of the contact interaction to the paramagnetic shift in lanthanide oxalates

It has been demonstrated by Lewis et al.[41] that within an isostructural series of lanthanide complexes, the Fermi-contact coupling constant A should remain the same from one element to another. In such situation, the isotropic contribution to the contact shift is given by[11]:

$$\delta_{contact} = \frac{A\,(g_J - 1)}{\hbar \mu_0 \mu_B g_J \gamma_I} \chi_{iso} \tag{8}$$

Given their isostructurality and the fact that their isotropic magnetic susceptibility is very similar (see table 2) neodymium and praseodymium oxalates have about the same contact shift contribution to their isotropic shift (within the 4% difference in isotropic susceptibility between the two species).

Experimental data show that the isotropic paramagnetic shifts of praseodymium and neodymium oxalates are strongly different (in the order of 200-300% depending on the carbon site, see table 3). Given the fact that contact contributions are similar in both compounds, this difference in isotropic shifts therefore proceeds from a very different dipolar contribution to the paramagnetic shift in both materials and characterizes a strong difference in their anisotropy of magnetic susceptibility.

Since paramagnetic shifts (-5 to + 8 ppm) in neodymium oxalate are much smaller than those observed in praseodymium oxalates (-12 to +25 ppm), there are two possible situations to explain the difference:

- either the contact shift contribution to the isotropic shift is important, and the pseudo-contact shift compensates it almost exactly for each nucleus by accident. In such situation, the anisotropy of magnetic susceptibility must be stronger in neodymium than in praseodymium oxalate (case 1: $\Delta\chi_{Pr} < \Delta\chi_{Nd}$)

- or the contact shift contribution is not important and, in such case, the only contribution to the isotropic paramagnetic shift is pseudo-contact. In such situation, the anisotropy of magnetic susceptibility must be stronger in praseodymium than in neodymium oxalate (case 2: $\Delta\chi_{Pr} > \Delta\chi_{Nd}$)

Another way to characterize differences in anisotropy of magnetic susceptibility comes by considering inhomogeneous linewidth. In a model initially proposed by Schwerk et al[42], Kubo, Spaniol and Terao[19] demonstrated that in paramagnetic systems, larger anisotropy of bulk magnetic susceptibility increased the field distribution in cylindrical powder samples resulting in the observation of broader lines. Their model gives an expression for the full-width-at-half-height (FWHH):

$$\mathrm{FWHH} = \left| 0.14 \frac{\chi_{iso}^{cell}}{V_{cell}} \times \Delta\chi \right| \tag{9}$$

Since the fitting of neodymium and praseodymium oxalates lines show gaussian linewidth of 4 ppm and 12 ppm respectively, we expect anisotropies of magnetic susceptibilities around 7 and 20% respectively. This shows that we are in the situation of case 2, and therefore that the contact contribution to the isotropic shifts is small in the case of oxalate lanthanides.

Comparison with magnetic measurements

Even though we could not test for anisotropy measurements with other methods, we had access to temperature-dependent SQUID measurements on our powder materials. This data gave us the isotropic macroscopic susceptibility as a function of temperature. The results of these measurements are available in the supplementary information.

With such data we could compare the isotropic component of the local magnetic susceptibility given by our newly developed NMR-based measurements with that obtained with

Table 2: Comparison of local isotropic magnetic susceptibilities from SQUID and NMR measurements for compounds **(2)** to **(4)**. Since the temperature measured for NMR experiments was 289K, the value reported from SQUID measurements are restrained to this temperature. The magnetic susceptibility curves from 2 to 300 K for all compounds are available in the SI.

Compound	χ_{iso}^{SQUID} ($\times 10^{-32}\,\mathrm{m}^3$)	χ_{iso}^{NMR} ($\times 10^{-32}\,\mathrm{m}^3$)
(2): $[Ce_2(C_2O_4)_3]$, 9.5 H_2O	4.769	4.784
(3): $[Pr_2(C_2O_4)_3]$, 9.5 H_2O	9.965	9.547
(4): $[Nd_2(C_2O_4)_3]$, 9.5 H_2O	10.36	10.27

SQUID measurements. In order to make this comparison, we assumed that the macroscopic magnetic susceptibility was the sum of the isotropic local component ("weak" paramagnetism approximation) and compared both values at the temperature at which the NMR experiments have been conducted.

We can see that the agreement is very good in all of the 3 cases. It is not perfect but slight discrepancies are to be expected as our temperature measurement on lead-nitrate showed some temperature gradient in our sample for the temperature conditions at which the NMR spectra were acquired.

This result confirms that the Fermi-contact component of the hyperfine interaction is negligible in this type of situation. This is a very significant result considering the fact that the compounds studied here have metal-centers from the first terms of the lanthanide series (which have the most diffuse f orbitals), and that the observed nuclei are only two bonds away from the metal center. In this situation, one could expect the Fermi-contact contribution to the hyperfine shift to be maximal. However, we show results that are high-quality and consistent with this simplified model despite the fact that we are using it in this disadvantageous situation. In addition to showing the robustness of that model, it gives high hopes for using this method on systems with bigger ligands and heavier lanthanide centers.

Resonance assignment

Table 3: Summary of resonance assignments for compounds **(2)** to **(4)**. The carbon labelling corresponds to that of the crystal data that can be found in the SI.

Compound	Carbon	δ_{iso}(/ppm)	$\Delta\delta$(/ppm)	η
(2)	C1	181.8	331.6	0.48
	C2	166.8	295.6	0.55
	C3	170.1	383.2	0.39
(3)	C1	197.0	698.4	0.37
	C2	161.6	612.5	0.48
	C3	190.7	810.5	0.32
(4)	C1	181.3	730.1	0.35
	C2	166.9	663.9	0.38
	C3	173.8	853.3	0.24

Finally, the last-but-not-least feat of this method is to give a direct assignment of NMR resonances within a paramagnetic material. Since paramagnetism scrambles the electronic density-based assignment that most chemists intuitively use on a daily basis, recovering fast-assignment capabilities in such systems is crucial.

Here, our fitting program calculates the chemical shift tensor parameters on the basis of the local magnetic properties for each nucleus, but the evaluation is made on the globality of the experimental data. Therefore, once the optimum spectrum is found, we just need to extract the chemical shift tensors of each nucleus in the asymmetric unit that were used to generate the best fit spectrum.

In each of the compounds **(2)** to **(4)**, we get the data that is presented in table 3. This shows that despite having chemical shifts that are too close to each other for the actual resolution in the experimental data, we can still isolate the isotropic shifts and shift anisotropies between nuclei that would be otherwise impossible to separate from the experiments.

Conclusion

This study shows that, by using the semi-empirical point-dipole approximation for the electronic magnetic tensor, it is possible to rapidly predict MAS NMR spectra of lanthanide-based paramagnetic species and use this fast prediction to search for an optimum for an

optimal magnetic susceptibility tensor.

This calculation proves to be very accurate in a difficult situation of NMR-observed nuclei in close proximity to the metal centers, high-density of paramagnetic centers within the crystal and working on a microcrystalline powder sample. Here, we presented our results on a relatively simple crystal structure (only 3 chemically inequivalent carbons) but we can expect this method to be applicable to bigger systems where, if the NMR data is accessible, a larger number of nuclei probing the local magnetic susceptibility could give more detailed information.

Large systems such as crystals with static disorder could also be accessible to fast-simulation processes and it could be possible to transform this local magnetic structure determination tool into an explorer of local static disorder within partially crystalline materials.

In order to apply this method in the future, we believe that the main challenge remains the experimental one. With paramagnetic systems, one can face short T_1, T_2 relaxation times or much larger anisotropies which hinder, in some cases, the recording of reliable NMR spectra.

It should be noted that prediction of solid-state NMR spectra thanks to our methodology is also very helpful to select the appropriate experimental parameters for the acquisition of NMR data for most lanthanide-based paramagnetic compounds.

Acknowledgements

The authors would like to thank the infrastructures that supported this research. In particular, the NMR and X-Ray diffraction platforms of the Université de Lorraine that allowed us to perform all the NMR and most of the X-Ray data acquisitions.

References

(1) Gukasov, A.; Brown, P. J. Determination of atomic site susceptibility tensors from polarized neutron diffraction data. *J. Phys. Condens. Matter* **2002**, *14*, 8831.

(2) Kibalin, I. A.; Yan, Z.; Voufack, A. B.; Gueddida, S.; Gillon, B.; Gukasov, A.; Porcher, F.; Bataille, A. M.; Morini, F.; Claiser, N.; *et al.*, Spin density in $YTiO_3$: I. Joint refinement of polarized neutron diffraction and magnetic x-ray diffraction data leading to insights into orbital ordering. *Phys. Rev. B* **2017**, *96*, 054426.

(3) Ridier, K.; Gillon, B.; Gukasov, A.; Chaboussant, G.; Cousson, A.; Luneau, D.; Borta, A.; Jacquot, J.-F.; Checa, R.; Chiba, Y.; *et al.*, Polarized neutron diffraction as a tool for mapping molecular magnetic anisotropy: local susceptibility tensors in CoII complexes. *Chem. Eur. J.* **2016**, *22*, 724–735.

(4) Salman, Z.; Giblin, S. R.; Lan, Y.; Powell, A. K.; Scheuermann, R.; Tingle, R.; Sessoli, R. Probing the magnetic ground state of the molecular dysprosium triangle with muon spin relaxation. *Phys. Rev. B* **2010**, *82*, 174427.

(5) Tesi, L.; Salman, Z.; Cimatti, I.; Pointillart, F.; Bernot, K.; Mannini, M.; Sessoli, R. Isotope effects on the spin dynamics of single-molecule magnets probed using muon spin spectroscopy. *Chem. Commun.* **2018**, *54*, 7826–7829.

(6) Gatteschi, D.; Barra, A. L.; Caneschi, A.; Cornia, A.; Sessoli, R.; Sorace, L. EPR of molecular nanomagnets. *Coord. Chem. Rev.* **2006**, *250*, 1514–1529.

(7) Walsh, J. P. S.; Sproules, S.; Chilton, N. F.; Barra, A.-L.; Timco, G. A.; Collison, D.; McInnes, E. J. L.; Winpenny, R. E. P. On the possibility of magneto-structural correlations: detailed studies of dinickel carboxylate complexes. *Inorg. Chem.* **2014**, *53*, 8464–8472.

(8) Balayssac, S.; Bertini, I.; Lelli, M.; Luchinat, C.; Maletta, M. Paramagnetic ions provide structural restraints in solid-state NMR of proteins. *J. Am. Chem. Soc.* **2007**, *129*, 2218–2219.

(9) Luchinat, C.; Parigi, G.; Ravera, E.; Rinaldelli, M. Solid-state NMR crystallography through paramagnetic restraints. *J. Am. Chem. Soc.* **2012**, *134*, 5006–5009.

(10) Kervern, G.; D'Aléo, A.; Toupet, L.; Maury, O.; Emsley, L.; Pintacuda, G. Crystal-structure determination of powdered paramagnetic lanthanide complexes by proton NMR spectroscopy. *Angew. Chem. Int. Ed.* **2009**, *48*, 3082–3086.

(11) Bertini, I.; Luchinat, C.; Parigi, G.; Ravera, E. *NMR of paramagnetic molecules: applications to metallobiomolecules and models*, 2nd ed.; Elsevier Science Ltd: Amsterdam, 2016.

(12) Parker, D.; Suturina, E. A.; Kuprov, I.; Chilton, N. F. How the ligand field in lanthanide coordination complexes determines magnetic susceptibility anisotropy, paramagnetic NMR shift, and relaxation behavior. *Acc. Chem. Res.* **2020**, *53*, 1520–1534.

(13) Harter, A. G.; Chakov, N. E.; Roberts, B.; Achey, R.; Reyes, A.; Kuhns, P.; Christou, G.; Dalal, N. S. Single-crystal ^{55}Mn NMR spectra of two Mn_{12} single-molecule magnets. *Inorg. Chem.* **2005**, *44*, 2122–2124.

(14) Kubo, T.; Nagano, A.; Goto, T.; Takeda, K.; Awaga, K. Comparison of ^{55}Mn NMR between two kinds of Mn_{12} molecular magnets: Mn_{12}Ac and Mn_{12}Ph. *J. Magn. Magn. Mater.* **2004**, *272-276*, E727–E729.

(15) Hansen, M. R.; Vosegaard, T.; Jakobsen, H. J.; Skibsted, J. ^{11}B chemical shift anisotropies in borates from ^{11}B MAS, MQMAS, and single-crystal NMR spectroscopy. *J. Phys. Chem. A* **2004**, *108*, 586–594.

(16) Walder, B. J.; Dey, K. K.; Davis, M. C.; Baltisberger, J. H.; Grandinetti, P. J. Two-dimensional NMR measurement and point dipole model prediction of paramagnetic shift tensors in solids. *J. Chem. Phys.* **2015**, *142*, 014201.

(17) De, S.; Tewary, S.; Garnier, D.; Li, Y.; Gontard, G.; Lisnard, L.; Flambard, A.; Breher, F.; Boillot, M.-L.; Rajaraman, G.; *et al.*, Solution and solid-state study of the spin-crossover [FeII(R-bik)$_3$](BF$_4$)$_2$ complexes (R = Me, Et, Vinyl). *Eur. J. Inorg. Chem* **2018**, *2018*, 414–428.

(18) De, S.; Flambard, A.; Garnier, D.; Herson, P.; Köhler, F. H.; Mondal, A.; Costuas, K.; Gillon, B.; Lescouëzec, R.; Le Guennic, B.; *et al.*, Probing the local magnetic structure of the [FeIII(Tp)(CN)$_3$]$^-$ building block via solid-state NMR spectroscopy, polarized neutron diffraction, and first-principle calculations. *Chem. Eur. J.* **2019**, *25*, 12120–12136.

(19) Kubo, A.; Spaniol, T. P.; Terao, T. The effect of bulk magnetic susceptibility on solid-state NMR spectra of paramagnetic compounds. *J. Magn. Reson.* **1998**, *133*, 330–340.

(20) Pell, A. J.; Pintacuda, G.; Grey, C. P. Paramagnetic NMR in solution and the solid state. *Prog. Nucl. Magn. Reson. Spectrosc.* **2019**, *111*, 1–271.

(21) Aleksis, R.; Pell, A. J. Separation of quadrupolar and paramagnetic shift interactions in high-resolution nuclear magnetic resonance of spinning powders. *J. Chem. Phys.* **2021**, *155*, 094202.

(22) Michaelides, A.; Skoulika, S.; Aubry, A. Crystal growth and structure of $La_2(C_20_4)_3$ 9.5H_20. *Mat. Res. Bull.* **1988**, *23*, 7.

(23) Dalal, P. V.; Saraf, K. B.; Shah, S. Growth of barium oxalate crystals in agar–agar gel and their characterization. *Cryst. Res. Technol.* **2009**, *44*, 36–42.

(24) Fung, B. M.; Khitrin, A. K.; Ermolaev, K. An improved broadband decoupling sequence for liquid crystals and solids. *J. Magn. Reson.* **2000**, *142*, 97–101.

(25) Kervern, G.; Pintacuda, G.; Emsley, L. Fast adiabatic pulses for solid-state NMR of paramagnetic systems. *Chem. Phys. Lett.* **2007**, *435*, 157–162.

(26) Guan, X.; Stark, R. E. A general protocol for temperature calibration of MAS NMR probes at arbitrary spinning speeds. *Solid State Nucl. Magn. Reson.* **2010**, *38*, 74–76.

(27) Hodgkinson, P.; Emsley, L. The reliability of the determination of tensor parameters by solid-state nuclear magnetic resonance. *J. Chem. Phys.* **1997**, *107*, 4808–4816.

(28) Pickard, C. J.; Mauri, F. All-electron magnetic response with pseudopotentials: NMR chemical shifts. *Phys. Rev. B* **2001**, *63*, 245101.

(29) Yates, J. R.; Pickard, C. J.; Mauri, F. Calculation of NMR chemical shifts for extended systems using ultrasoft pseudopotentials. *Phys. Rev. B* **2007**, *76*, 024401.

(30) Clark, S. J.; Segall, M. D.; Pickard, C. J.; Hasnip, P. J.; Probert, M. I. J.; Refson, K.; Payne, M. C. First principles methods using CASTEP. *Z. Kristallogr. Cryst. Mater.* **2005**, *220*, 567–570.

(31) Perdew, J. P.; Burke, K.; Ernzerhof, M. Generalized gradient approximation made simple. *Phys. Rev. Lett.* **1996**, *77*, 3865–3868.

(32) Mondal, A.; Gaultois, M. W.; Pell, A. J.; Iannuzzi, M.; Grey, C. P.; Hutter, J.; Kaupp, M. Large-scale computation of nuclear magnetic resonance shifts for paramagnetic solids using CP2K. *J. Chem. Theory Comput.* **2018**, *14*, 377–394.

(33) Clément, R. J.; Pell, A. J.; Middlemiss, D. S.; Strobridge, F. C.; Miller, J. K.; Whittingham, M. S.; Emsley, L.; Grey, C. P.; Pintacuda, G. Spin-transfer pathways in paramagnetic lithium transition-metal phosphates from combined broadband isotropic

solid-state MAS NMR spectroscopy and DFT calculations. *J. Am. Chem. Soc.* **2012**, *134*, 17178–17185.

(34) Gendron, F.; Sharkas, K.; Autschbach, J. Calculating NMR chemical shifts for paramagnetic metal complexes from first-principles. *J. Phys. Chem. Lett.* **2015**, *6*, 2183–2188.

(35) Furet, E.; Costuas, K.; Rabiller, P.; Maury, O. On the sensitivity of f electrons to their chemical environment. *J. Am. Chem. Soc.* **2008**, *130*, 2180–2183.

(36) Suturina, E. A.; Kuprov, I. Pseudocontact shifts from mobile spin labels. *Phys. Chem. Chem. Phys.* **2016**, *18*, 26412–26422.

(37) Clavaguéra, C.; Dognon, J.-P.; Pyykkö, P. Calculated lanthanide contractions for molecular trihalides and fully hydrated ions: the contributions from relativity and $4f$-shell hybridization. *Chem. Phys. Lett.* **2006**, *429*, 8–12.

(38) Orton, H. W.; Huber, T.; Otting, G. Paramagpy: software for fitting magnetic susceptibility tensors using paramagnetic effects measured in NMR spectra. *Magn. Reson.* **2020**, *1*, 1–12.

(39) Paquin, R.; Pelupessy, P.; Duma, L.; Gervais, C.; Bodenhausen, G. Determination of the antisymmetric part of the chemical shift anisotropy tensor via spin relaxation in nuclear magnetic resonance. *J. Chem. Phys.* **2010**, *133*, 034506.

(40) van Meerten, S. G. J.; Franssen, W. M. J.; Kentgens, A. P. M. ssNake: a cross-platform open-source NMR data processing and fitting application. *J. Magn. Reson.* **2019**, *301*, 56–66.

(41) Lewis, W. B.; Jackson, J. A.; Lemons, J. F.; Taube, H. Oxygen-17 NMR Shifts in Aqueous Solutions of Rare-Earth Ions. *The Journal of Chemical Physics* **1962**, *36*, 694–701.

(42) Schwerk, U.; Michel, D.; Pruski, M. Local Magnetic Field Distribution in a Polycrystalline Sample Exposed to a Strong Magnetic Field. *Journal of Magnetic Resonance, Series A* **1996**, *119*, 157–164.

Graphical TOC Entry